Journal of Power Sources 258 (2014) 134–141

Contents lists available at ScienceDirect

Journal of Power Sources

journal homepage: www.elsevier.com/locate/jpowsour

A NiFeCu alloy anode catalyst for direct-methane solid oxide fuel cells

Wei Wang [a], Huaiyu Zhu [a], Guangming Yang [a], Hee Jung Park [b], Doh Won Jung [b], Chan Kwak [b,1], Zongping Shao [a,*]

[a] State Key Laboratory of Materials-Oriented Chemical Engineering, College of Chemistry & Chemical Engineering, Nanjing University of Technology, No. 5 Xin Mofan Road, Nanjing 210009, PR China
[b] Samsung Advanced Institute of Technology (SAIT), 14-1 Nongseo-dong, Yongin-si, Gyunggi-do 446-712, Republic of Korea

HIGHLIGHTS

- NiFeCu alloy catalysts were prepared by three different methods.
- NiFe–ZrO_2/Cu (IMP) catalyst showed highest coking resistance toward methane.
- High power output of 1165 mW cm^{-2} was obtained with CH_4–O_2 as fuel at 850 °C.
- The fuel cell with this NiFe–ZrO_2/Cu (IMP) catalyst layer delivered good stability.

ARTICLE INFO

Article history:
Received 23 December 2013
Received in revised form
17 January 2014
Accepted 3 February 2014
Available online 12 February 2014

Keywords:
Solid oxide fuel cells
Anode catalyst layer
Copper-containing alloy
Partial oxidation of methane
Preparation methods

ABSTRACT

In this study, a new anode catalyst based on a NiFeCu alloy is investigated for use in direct-methane solid oxide fuel cells (SOFCs). The influence of the conductive copper introduced into the anode catalyst layer on the performance of the SOFCs is systematically studied. The catalytic activity for partial oxidation of methane and coking resistance tests are proposed with various anode catalyst layer materials prepared using different methods, including glycine nitrate process (GNP), physical mixing (PM) and impregnation (IMP). The surface conductivity tests indicate that the conductivities of the NiFe–ZrO_2/Cu (PM) and NiFe–ZrO_2/Cu (IMP) catalysts are considerably greater than that of NiFe–ZrO_2/Cu (GNP), which is consistent with the SEM results. Among the three preparation methods, the cell containing the NiFe–ZrO_2/Cu (IMP) catalyst layer performs best on CH_4–O_2 fuel, especially under reduced temperatures, because the coking resistance should be considered in real fuel cell conditions. The cell containing the NiFe–ZrO_2/Cu (IMP) catalyst layer also delivers an excellent operational stability using CH_4–O_2 fuel for 100 h without any signs of decay. In summary, this work provides new alternative anode catalytic materials to accelerate the commercialization of SOFC technology.

1. Introduction

A chemical bond is one of the most effective methods of energy storage, and chemicals that are rich in high-energy bonds have been widely used as fuels. To release the chemical energy stored in the bonds, chemical or electrochemical reactions must be conducted. Combustion is the simplest way to release chemical energy in the form of heat. In many applications, electrical power is preferred because it is much more flexible and manageable. In a commercial fire power plant, the chemical energy is first converted to mechanical energy using combustion engines, and then the mechanical energy is further converted to electric power. This process is applied widely for the generation of electric power from fuels; however, it is limited by the Carnot cycle and its low energy conversion efficiency is unavoidable.

Fuel cells are a type of energy conversion device that can release chemical energy directly into electric power without any intermediate processes, allowing the energy conversion efficiency to be twice as high as that of a combustion engine. Thus, over the past decades, rapidly expanding research activities on fuel cells have been carried out. One significant advantage of solid oxide fuel cells (SOFCs) over the low-temperature fuel cells is fuel flexibility because the high operation temperature facilitates the cleavage of chemical bonds to release chemical energy. Thus, in addition to

* Corresponding author. Tel.: +86 25 83172256; fax: +86 25 83172242.
E-mail addresses: c.kwak@samsung.com (C. Kwak), shaozp@njut.edu.cn (Z. Shao).
[1] Tel.: +82 31 280 6721; fax: +82 31 280 6739.

http://dx.doi.org/10.1016/j.jpowsour.2014.02.008
0378-7753/

hydrogen, various stable fuels, such as hydrocarbons, ammonia, carbon monoxide and even solid carbon, can be used as potential fuels for SOFCs [1–5]. When compared to gasoline and coal, natural gas (methane) is much cleaner; therefore, natural gas as a fuel has recently attracted increasing attention. In particular, methane-fueled SOFCs are believed to potentially reduce emissions and increase fuel efficiency [6–10].

State-of-the-art SOFC anodes are Ni–YSZ cermets, which are prone to coke formation when operating on carbon-containing fuels, because Ni is a good catalyst for the cracking of hydrocarbons. Over the past decades, considerable research efforts have been directed towards the development of innovative non-nickel-based anodes [11,12]. However, the performances of these anodes are still not satisfactory. To date, the conventional Ni cermet anodes are the preferred choice for practical applications because of their low cost, high electronic conductivities, reasonable ionic conductivities, high stability under reducing atmospheres and high operational temperatures, moderate thermal expansion coefficient that matches well with that of the YSZ electrolyte and high electrocatalytic activity. The key to realizing the successful operation of Ni-based cermet anodes on carbon-containing fuels is to increase their coking resistance.

Modifying the outer surface of conventional Ni-based cermet anodes with a catalyst layer of high activity for the steam/carbon dioxide reforming reaction, partial oxidation of hydrocarbons and good resistance towards coke formation is one of the simplest ways to increase the operational stability and performance of hydrocarbon-fueled SOFCs [13–15]. Barnett and Zhan first adopted this concept and deposited a thin Ru–CeO_2 layer onto the outer surface of a Ni–YSZ anode for the reforming of hydrocarbons into syngas [13]. The excellent coking resistance of Ru–CeO_2 permitted the cells to operate in an internal reforming mode with a wider range of fuels. However, the high price and poor thermo-mechanical compatibility with nickel-cermet anodes during thermal and redox cycling of Ru–CeO_2 make it less attractive in practical applications [16].

In our previous study, NiFe–ZrO_2 alloy catalysts were synthesized and investigated for the anode catalyst layer for partial oxidation of methane in SOFCs [17]. However, all of those catalysts (Ru–CeO_2 and NiFe–ZrO_2) displayed poor conductivity, introducing serious current collecting problems, which would limit them from use in fuel cells for practical applications. The electrical conductivity can be substantially improved with the addition of proper amounts of inert metallic copper [18]. As a result, high power output and superior coking resistance are obtained with the copper-incorporated catalysts. Additionally, the preparation method may also have significant effects on the performance of a catalyst [19]. It is therefore worthwhile to understand how the conductive copper introduced into the anode catalyst layer influences the performance of the catalyst. In this study, several methods of introducing copper into the NiFe–ZrO_2 catalyst were explored, and their effects on the catalytic activity for methane conversion, coking resistance and particularly on cell performance operating on methane fuel were systematically investigated.

2. Experimental

2.1. Synthesis and fabrication

To synthesize the NiFe–ZrO_2 catalyst powders with a composition of 24 wt.% Ni, 6 wt.% Fe and balanced by ZrO_2, primary products were first obtained via a glycine–nitrate solution combustion technique [17]. The as-obtained primary powders were further calcined at 850 °C in static air for 5 h to obtain the desired catalysts. To improve the electrical conductivity to be more suitable for fuel cell applications, 50 wt.% copper was added to the NiFe–ZrO_2 catalyst. Three methods for the introduction of copper into the catalyst were adopted. First, copper in the form of $Cu(NO_3)_2$ (Sinopharm chemical reagents Co., Ltd., China) was introduced during the solution combustion stage, and the final product was named NiFe–ZrO_2/Cu (GNP), with a composition of 12 wt.% Ni, 3 wt.% Fe, 50 wt.% Cu and balanced ZrO_2. Second, the NiFe–ZrO_2/Cu composite catalyst was prepared by physical mixing (PM) of the as-prepared NiFe–ZrO_2 catalyst, by solution combustion, and copper oxide (CuO) powder via hand grinding with the help of an agate mortar and pestle. The weight ratio of NiFe–ZrO_2 to copper was 1:1. After physical mixing, the catalysts were further calcined at 850 °C in static air for 5 h. This catalyst was labeled NiFe–ZrO_2/Cu (PM). Third, an impregnation process (IMP) was used to introduce copper to the NiFe–ZrO_2 catalyst, and the as-obtained catalyst was labeled NiFe–ZrO_2/Cu (IMP). For a typical synthesis, a proper amount of copper nitrate solution was first slowly impregnated into the NiFe–ZrO_2 catalyst powder with stirring for several times to achieve the required copper content and then aged at room temperature for 5 h. After drying, the catalyst was calcined at 850 °C in static air for 5 h. For catalytic performance and carbon deposition tests, the catalyst powders were pressed into disk-shaped pellets and then crushed into 40–60 mesh grains.

The fuel cells applied in this study were composed of a $La_{0.8}Sr_{0.2}MnO_3$ (LSM) cathode, a $(Y_2O_3)_{0.1}(ZrO_2)_{0.9}$ (YSZ) electrolyte and a NiO + YSZ anode (NiO:YSZ = 60:40, by weight). The LSM cathode material was synthesized using a combined EDTA-citrate complexation sol–gel process with metal nitrates (analytical reagents) as the cation sources [20]. NiO and YSZ are commercial products obtained from a suitable supplier (Chengdu Shudu Nano-science Co., Ltd. and Tosoh, respectively). To fabricate the fuel cells, disk-shaped anode substrates were prepared using a tape-casting technique. Detailed information about the fabrication of the three-layer single cell can be found in our previous work [18]. The dimensions of the three SOFC cells are 11 mm in diameter after calcined at 1400 °C. The porosities of the three SOFC cells are about 40% after the hydrogen reduction process. To prepare the catalyst layer, a slurry of the catalyst powder was prepared and was then screen-painted onto the outer surface of the anode layer and sintered at 850 °C for 1 h. In the stability test, a mesh-like morphological structure of silver paste was placed via a stick directly onto the LSM cathode surface to create the current collector and then fired at 180 °C for 1 h.

2.2. Catalytic evaluation

The catalytic activity of the various catalysts was tested in a flow-through type fixed-bed quartz-tube reactor with an inner diameter of ~8 mm. Approximately 0.2 g of 40–60 mesh catalyst particles were located in the middle section of the reactor. For catalytic partial oxidation of methane test, a gas mixture composed of CH_4, O_2 and He at a molar ratio of 2:1:16 and a total flow rate of 95 mL min^{-1} [STP] was introduced from the top of the reactor and controlled with the help of AFC 80MD digital mass flow controllers (Qualiflow). Compositional analysis of the effluent gases from the bottom of the reactor was performed using a Varian 3800 gas chromatograph, which was equipped with a Hayesep Q, a Poraplot Q, a 5 Å molecular sieve capillary column and a thermal conductivity detector (TCD) for the separation and detection of H_2, O_2, CO, CO_2 and CH_4. The catalytic reactions were performed at 600–850 °C. The calculation methods of methane conversion and CO selectivity were described specifically in our previous work [21].

2.3. Characterization

The phase structure of the various samples was examined using an X-ray diffractometer (XRD, D8 Advance, Bruker, Germany) with Cu Kα radiation (λ = 0.1541 nm). Hydrogen temperature-programmed reduction (H_2-TPR) was used to identify the chemical interaction between the nickel phase and the support [21], while oxygen temperature-programmed oxidization (O_2-TPO) was used to test the coking resistance of the various catalysts [21]. The *I–V* and *I–P* polarization curves of the fuel cells, tested in 4-probe mode at 650–850 °C, were obtained using a Keithley 2420 source meter. During the measurements, hydrogen or CH_4–O_2 gas mixtures were fed into the anode chamber while ambient air was supplied as the oxidant gas to the cathode chamber. The flow rates of hydrogen and methane were maintained at 80 mL min^{-1} [STP]. Morphologies of the different catalyst layers were observed by a field emission scanning electron microscopy (FESEM, JEOL-S4800).

The surface conductivity of the catalysts was measured in hydrogen at 850 °C using the 4-probe DC method. Silver paste was painted onto the surface of the catalyst layer (separated by a distance of S) to form current and voltage electrodes. Two silver wires were used as voltage contacts and attached to the electrodes with silver paste. Alternatively, the other silver wires were used as current contacts. A constant current was applied to the current wires, and the responses of the voltage wires were recorded with a Keithley 2420 source meter. The conductivity was calculated as follows:

$$\rho = \frac{I}{2\pi SV} \quad (1)$$

where ρ is the conductivity (S cm^{-1}), S is the distance between the probes (cm), V is the voltage (V), and I is the current (A) [22].

3. Results and discussion

3.1. Basic properties

It is well known that copper oxide can form a solid solution with other metal oxides. In fact, the mutual dissolve among copper oxide, nickel oxide and iron oxide is very flexible; thus, a wide range of solid solutions or composite oxides can form, as reported in the literature [23,24]. Additionally, metallic copper may also form alloys with other metals, such as nickel and iron. Different preparation methods may result in different phase compositions of the NiFe–ZrO_2/Cu catalysts, thereby affecting the catalytic activity and coking resistance properties.

To examine the role that the preparation method had on the phase composition of NiFe–ZrO_2/Cu catalysts, both the unreduced and reduced catalysts prepared using the three different aforementioned methods were examined by XRD, and the corresponding patterns are shown in Fig. 1a (unreduced) and Fig. 1b (reduced). The XRD patterns of the copper-free NiFe–ZrO_2 catalyst are also presented for comparison. For the unreduced copper-free catalyst prepared using the solution combustion technique, five phases were observed in the catalyst: monoclinic ZrO_2 phase, NiO, $Ni_xFe_{3-x}O_4$ spinel-type composite oxide, Fe_2O_3 and Fe_3O_4. When copper was introduced to all three catalysts, in addition to ZrO_2, NiO and $Ni_xFe_{3-x}O_4$, new phases of CuO and a $Cu_{0.2}Ni_{0.8}O_2$-type solid solution were observed. This result suggests that the copper oxide likely reacted partially with the nickel in the catalysts to form a new CuO–NiO solid solution. Because the catalysts are composed of much higher concentrations of copper (50 wt.%) than nickel (12 wt.%), the catalyst should have poorer activity for methane oxidation/reforming but lower coke formation. The depletion of

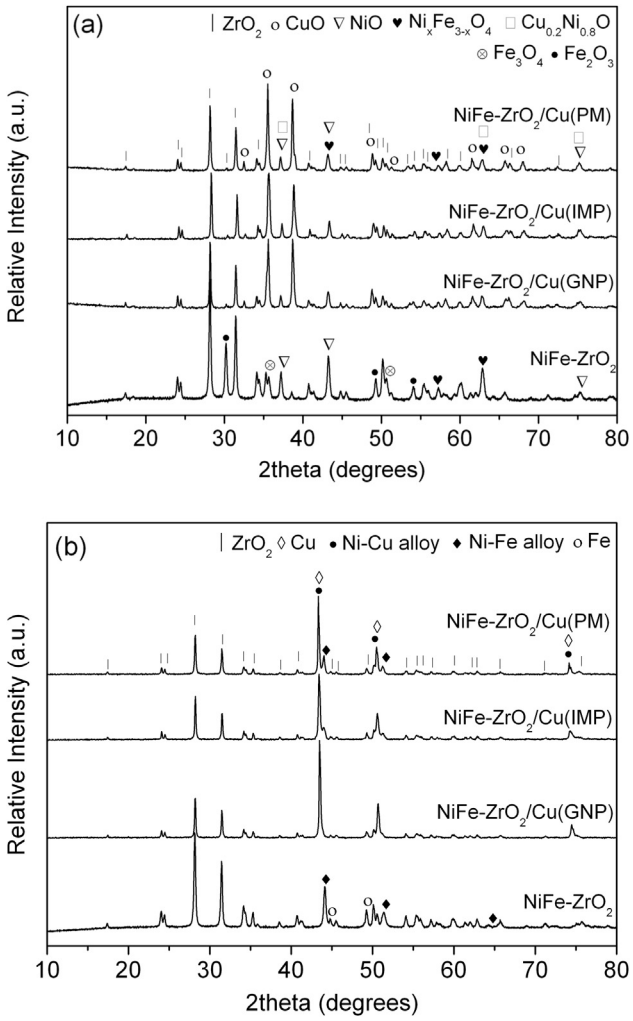

Fig. 1. XRD patterns of the various NiFe–ZrO_2/Cu catalysts before and after the hydrogen reduction at 850 °C.

nickel from the nickel catalysts and the dissolution into the copper may have unfavorable effects on the catalytic activity of the catalysts. Because of the multi-phases within the catalysts, it is difficult to precisely compare the concentrations for the various species. However, from Fig. 1a, it is clear that the peak intensity of CuO in the NiFe–ZrO_2/Cu (PM) catalyst is noticeably higher than for the other two catalysts. This result suggests that the interaction between CuO and the NiFe–ZrO_2 catalyst was weakest for the sample prepared using the physical mixing/calcination method. This is easily understood because the solid–solid reaction required the highest energy because of the diffusion block.

Fig. 1b presents the XRD patterns of the various catalysts after the reduction by hydrogen at 850 °C. Diffraction peaks at 2θ values of 43.3°, 50.5° and 74.2° in the XRD patterns of all three copper-containing samples can be assigned to the diffraction planes of (111), (200) and (220) of the Ni–Cu alloy. This result suggests the formation of a Ni–Cu alloy in the reduced catalysts, which is consistent with the observation of the NiO–CuO solid solution in the unreduced catalysts. Interestingly, a Ni–Fe alloy appeared for the catalysts prepared via IMP and PM, while the peak intensity of this alloy was less pronounced in the XRD patterns of catalysts prepared using GNP. For the copper-incorporated catalysts prepared by PM and IMP, the copper-free NiFe–ZrO_2 catalysts were first prepared; thus, the Ni–Fe alloy was formed before the

introduction of copper. For NiFe–ZrO_2/Cu (GNP), all of the raw materials, including copper, nickel, iron and zirconia, were prepared in a mixed solution during the solution combustion synthesis. Because the various raw materials were homogeneously mixed on the atomic level, the diffusion resistance required for the formation of NiO–CuO solid solution is negligible. Because much higher concentrations of copper ions than iron ions were present in the mixed solution, the formation of the NiO–CuO solid solution was preferred over the NiO–FeO solid solution. This resulted in the NiFe alloy being less favored after reduction.

Chemical interactions between different species in the catalysts were characterized by hydrogen temperature-programmed reduction (H_2-TPR) and the corresponding profiles are shown in Fig. 2. According to the literature, two types of reduction peaks may be observed in the H_2-TPR profiles of CuO, located at 220–260 °C and 330 °C, which were assigned to the reduction of highly dispersed CuO and bulk CuO, respectively [25], while the reduction of free or unsupported NiO occurred at a temperature of approximately 330 °C [26]. Thus, the reduction peaks at 220–240 °C can be assigned to the reduction of the highly dispersed CuO in the catalysts. It was found that the amount of such highly dispersed CuO was strongly dependent on the preparation methods. The lowest peak temperature (220 °C) and the narrowest peak suggested that the copper was most highly dispersed in the catalyst prepared by GNP because of the atomic level homogenous mixing of the copper in the combustion solution stage. The reduction peaks at approximately 330 °C were assigned to the simultaneous reduction of bulk CuO and NiO. For the NiFe–ZrO_2/Cu (GNP) catalyst, the reduction peak was much weaker than those in the catalysts prepared by IMP and PM, suggesting that both NiO and CuO had much stronger interactions with ZrO_2 in the catalyst prepared using the solution combustion technique. These results showed that multiple reduction peaks above 500 °C in the H_2-TPR profile appeared only for the NiFe–ZrO_2/Cu (GNP) catalyst prepared using the solution combustion technique.

3.2. Catalytic performance and carbon deposition

Fig. 3 shows the methane conversion and CO selectivity of the copper-incorporated catalysts for the partial oxidation of the methane reaction at 600–850 °C with a methane-to-oxygen ratio of 2:1. From Fig. 3a, it was found that the different synthesis methods could directly affect the catalytic activity. For example, the

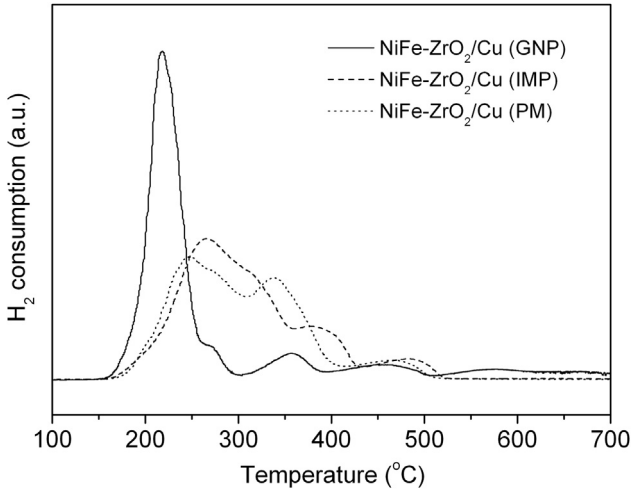

Fig. 2. H_2-TPR profiles of the various NiFe–ZrO_2/Cu catalysts.

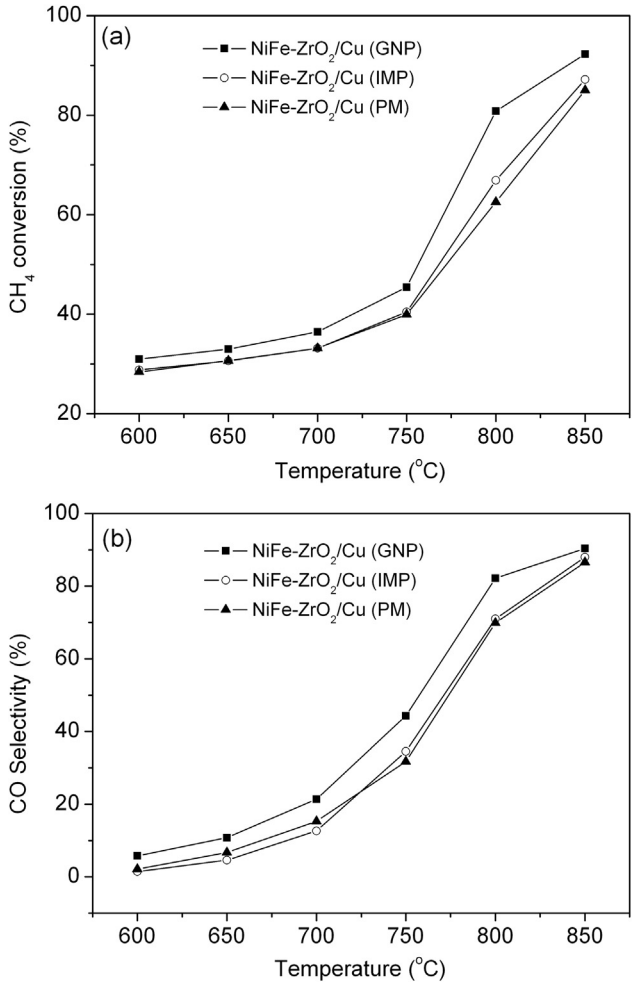

Fig. 3. CH_4 conversion (a) and CO selectivity (b) of the NiFe–ZrO_2/Cu (GNP), NiFe–ZrO_2/Cu (IMP) and NiFe–ZrO_2/Cu (PM) catalysts for the partial oxidation of methane (CH_4:O_2 = 2:1).

methane conversions at 850 °C for the NiFe–ZrO_2/Cu (GNP), NiFe–ZrO_2/Cu (PM) and NiFe–ZrO_2/Cu (IMP) catalysts were 92.2%, 85.0% and 87.1%, respectively. The catalyst prepared using GNP exhibited a superior catalytic activity for methane conversion than the other two catalysts. When the operational temperature decreased to the range of 750–800 °C, the methane conversion dropped sharply for all three catalysts. However, when the temperature decreased below 700 °C, the three catalysts presented similar activities for methane conversion. For example, the methane conversions were 33.0%, 30.6% and 30.6% for the NiFe–ZrO_2/Cu (GNP), NiFe–ZrO_2/Cu (PM) and NiFe–ZrO_2/Cu (IMP) catalysts at 650 °C, respectively. Fig. 3b displays the CO selectivity of the three catalysts for the partial oxidation of the methane reaction at 600–850 °C. At high operating temperatures, all of the catalysts showed good CO selectivity. For example, at 850 °C, the CO selectivities were 90.4%, 86.5% and 88.0% for the NiFe–ZrO_2/Cu (GNP), NiFe–ZrO_2/Cu (PM) and NiFe–ZrO_2/Cu (IMP) catalysts, respectively. However, the decrease in reaction temperature led to a reduced CO selectivity, especially for the catalysts prepared by IMP and PM. In fact, the main reaction that occurred for the catalysts prepared by IMP and PM at 600 °C was the methane deep oxidation reaction. In our previous work, the Ni4Fe1–ZrO_2 catalyst showed excellent catalytic activity for the partial oxidation of methane at temperatures above 650 °C [17]. However, in this study, the addition of copper

could sharply decrease the catalytic activity, especially at lower temperatures. It was reported that the addition of a small amount of copper (5–7 wt.%) could improve the catalytic activity of Ni-based catalysts [27]. However, the addition of excess copper could lead to a decrease in the catalytic activity because the excess copper could cover the active sites on the surface of the catalyst [18]. Thus, during this study, the addition of 50 wt.% Cu to the catalyst led to a lower catalytic activity for the partial oxidation of methane. However, when the catalyst was applied as the anode catalyst layer of a fuel cell, a sufficient amount of copper was required to maintain high electrical conductivity. The electrical conductivity of the catalysts will be discussed later in this study.

A key criterion for evaluating an anode catalyst layer is its resistance towards coke formation. Previously, we have demonstrated that carbon deposition onto Ni4Fe1–ZrO_2 showed best coking resistance when compared to the pure Ni–ZrO_2 and pure Fe–ZrO_2 catalysts in the same conditions [17]. Thus, the influence of different preparation methods on the carbon deposition behavior of the various copper-containing catalysts was investigated by treatment of the catalyst under a stream of pure methane at 850 °C for 5 min, followed by oxygen temperature-programmed oxidization (O_2-TPO) analysis on the spent catalysts. The results of the analysis are shown in Fig. 4. After treatment at 850 °C, the areas of the CO_2 peak for the NiFe–ZrO_2/Cu (GNP), NiFe–ZrO_2/Cu (PM) and NiFe–ZrO_2/Cu (IMP) catalysts were 2.16×10^{-6}, 2.50×10^{-6} and 8.95×10^{-7}, respectively. These results indicated that NiFe–ZrO_2/Cu (IMP) exhibited superior coking resistance compared to the other two catalysts. This result likely occurred because the copper that covered the nickel surface reduced the contact of nickel with methane, and thus decreased the coke formation rate, as well as the catalytic activity.

3.3. Surface conductivity

As previously mentioned, high electrical conductivity is important in many applications and good cell performance can be associated with high electrical conductivity. Thus, the surface conductivity of the various NiFe–ZrO_2/Cu catalyst layers was measured by applying the 4-probe DC method at 850 °C in a hydrogen atmosphere. It was reported that the minimum volumetric percentage required to form a percolative phase in a composite was approximately 16 vol.% [28,29]. In the proposed NiFe–ZrO_2/Cu catalyst, the estimated volumetric percentage of metallic copper was approximately 42%, which is considerably higher than the aforementioned threshold. Thus, in principle, all of the three copper-containing catalysts could present considerable surface conductivities. However, the preparation methods could dramatically affect the surface conductivity properties, the results of which are provided in Table 1. For comparison, the surface conductivity of a Ni–YSZ cermet anode is also presented. The values of the surface conductivities of the NiFe–ZrO_2/Cu (GNP), NiFe–ZrO_2/Cu (PM) and NiFe–ZrO_2/Cu (IMP) layers were 4.65, 10.4 and 9.19 S cm^{-1}, respectively. Alternatively, the surface conductivity of the Ni–YSZ cermet anode was 12.3 S cm^{-1}, which was nearly identical to the values of the NiFe–ZrO_2/Cu (PM) and NiFe–ZrO_2/Cu (IMP) samples. Because the traditional Ni–YSZ anodes are good current collectors for SOFCs, the results of the present study indicated that the copper formed a percolate phase in the catalyst layers prepared by PM and IMP and that these two samples could be used as the current collector under actual fuel cell conditions. The excellent conductivity of the NiFe–ZrO_2/Cu (PM) and NiFe–ZrO_2/Cu (IMP) catalysts promotes their wide adoption as the anode catalyst layer in SOFCs.

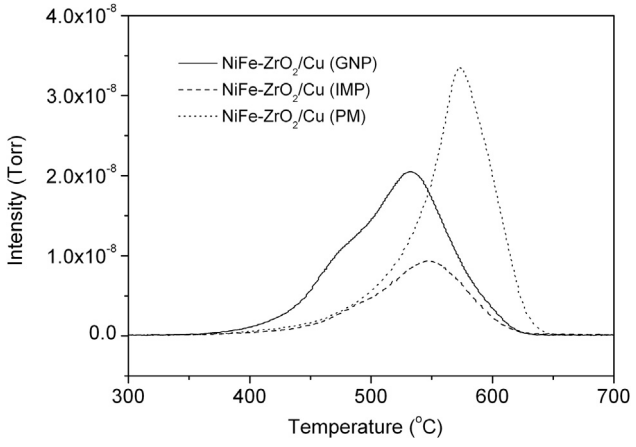

Fig. 4. O_2-TPO profiles of the NiFe–ZrO_2/Cu (GNP), NiFe–ZrO_2/Cu (IMP) and NiFe–ZrO_2/Cu (PM) catalysts after treatment in pure methane for 5 min at 850 °C.

3.4. Performance in actual cells

The as-prepared catalysts were further applied as anode catalyst layers in actual fuel cells. Fig. 5 shows the SEM images of the catalyst layers, after hydrogen reduction, from the surface view. Fig. 5a & b, c & d and e & f are the SEM images for NiFe–ZrO_2/Cu (GNP) NiFe–ZrO_2/Cu (IMP) and NiFe–ZrO_2/Cu (PM), respectively. As shown in Fig. 5, we found that small metal particles approximately 50 nm in diameter were dispersed on the surface of the catalyst. However, the catalyst layer prepared by IMP and PM had a much better dispersion for these small metal particles. Thus, the metal particles in the catalyst layer prepared by the IMP and PM methods formed a better percolative route than those prepared using the GNP method. The SEM results agree well with the surface conductivity results. The impact of the catalyst layer on the cell performance was first evaluated by operating with hydrogen fuel. Under operation on with hydrogen fuel, the catalytic activity and coking resistance of the catalyst layer were less significant on the cell power output, while the cell performance was mainly affected by its conductivity and gas diffusion properties. Fig. 6 displays the *I–V* and *I–P* curves of fuel cells with the various catalyst layers operating on hydrogen at different temperatures. The cell with the NiFe–ZrO_2/Cu (GNP) catalyst layer delivered peak power densities (PPDs) of 1159, 940, 699, 444 and 248 mW cm^{-2} at 850, 800, 750, 700 and 650 °C, respectively (Fig. 6a). By applying the NiFe–ZrO_2/Cu (IMP) and NiFe–ZrO_2/Cu (PM) catalyst layers, PPDs of 1238 (Fig. 6b) and 1103 mW cm^{-2} (Fig. 6c) were obtained at 850 °C for the cells, respectively. No obvious concentration polarization was observed at high current density and various temperatures for all three cells with different catalyst layers. This result indicates that the NiFe–ZrO_2/Cu catalyst layers performed well with sufficient porosity. The high power output also suggests the sufficient electric conductivity of the catalyst layers after the incorporation of 50 wt.% copper.

The various cells were further subjected for operation with a methane–oxygen gas mixtures with a methane-to-oxygen ratio of

Table 1
Surface conductivity values for various samples using the four-point surface conductivity probes in hydrogen atmosphere at 850 °C.

Sample	Surface conductivity (S cm^{-1})
NiFe–ZrO_2/Cu (GNP)	4.65
NiFe–ZrO_2/Cu (PM)	10.4
NiFe–ZrO_2/Cu (IMP)	9.19
Ni–YSZ	12.3

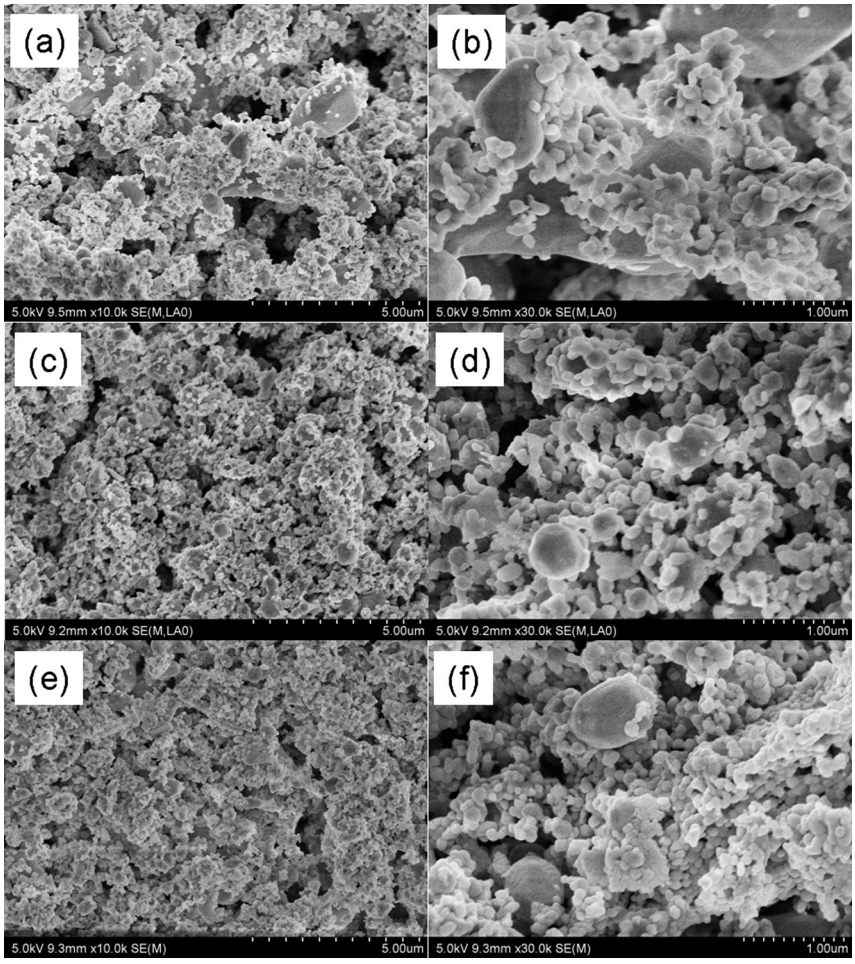

Fig. 5. SEM images of the surface of the various anode catalyst layers after hydrogen reduction. (a & b): NiFe–ZrO_2/Cu (GNP), (c & d): NiFe–ZrO_2/Cu (IMP) and (e & f): NiFe–ZrO_2/Cu (PM).

4:1. For a typical methane partial oxidation, the methane-to-oxygen ratio should be 2:1; herein, the methane rich condition was applied to accelerate coke formation over the fuel cell anode to further evaluate the tolerance of carbon deposition. Relatively stable performance was achieved for all three cells with different catalyst layers. Fig. 7 presents the corresponding *I*–*V* and *I*–*P* polarization curves. The cell that contained the NiFe–ZrO_2/Cu (GNP) catalyst layer delivered PPDs of 1080, 800, 561, 335 and 155 mW cm^{-2} at 850, 800, 750, 700 and 650 °C, respectively, which were only slightly lower than those operating with hydrogen fuel. This demonstrated that the catalyst layer had sufficient catalytic activity for the methane partial oxidation and CO_2/H_2O reforming. For the cells that contained the other two catalysts layers, comparable cell performance was also obtained at high temperature. For example, PPDs of 1011 and 1165 mW cm^{-2} were obtained at 850 °C for the cells with the NiFe–ZrO_2/Cu (PM) and NiFe–ZrO_2/Cu (IMP) catalysts layers, respectively. At lower operating temperatures, the difference in power outputs among the three cells became more obvious. For example, the PPDs of the fuel cells with NiFe–ZrO_2/Cu (GNP), NiFe–ZrO_2/Cu (PM) and NiFe–ZrO_2/Cu (IMP) catalyst layers that utilized methane–oxygen fuel at 650 °C were 155, 200 and 334 mW cm^{-2}, respectively. Thus, NiFe–ZrO_2/Cu (IMP) is more promising for SOFCs operated at low temperature. According to the results in Fig. 3, the three catalysts had comparable activity for methane conversion and CO selectivity at 650 °C. Thus, the difference in power output at 650 °C should not be a result of their catalytic activity.

Under the actual fuel cell test conditions, in addition to their performance as a catalyst for fuel reforming, the catalyst layer also performed as a gas diffusion layer to protect the anode from being exposed directly in the hydrocarbon fuels. A good coking resistance of the catalyst layer was a critical element in maintaining its good mechanical integrity during the operation and also protected the anode from the direct exposure to hydrocarbons, thereby suppressing coke formation. The variation in power outputs of the cells at 650 °C likely related to the different coking resistances of the various catalysts. We then further studied the coking resistance of the various catalysts towards methane by first treating the various catalysts under a pure methane atmosphere at 650 °C for 5 min. The catalysts were then subjected to O_2-TPO analysis, the profiles of the CO_2 signal are shown in Fig. 8. The NiFe–ZrO_2/Cu (IMP) catalyst had much superior coking resistance than the other two catalysts, which was indicated by much smaller CO_2 peak area. The amount of carbon deposited on the NiFe–ZrO_2/Cu (IMP) catalyst was only 30.0% and 19.0% of those on the NiFe–ZrO_2/Cu (GNP) and NiFe–ZrO_2/Cu (PM) catalysts, respectively. As shown in Fig. 9, the fuel cells with NiFe–ZrO_2/Cu (IMP) catalyst layer also delivered a good operational stability without any degradation for approximately 100 h of operation on methane–oxygen gas mixtures under the certain current density of 250 mA cm^{-2} at 650 °C. A current density of 250 mA cm^{-2} was used to maintain the cell voltage at around 0.7 V, which is beneficial to the practical applications. The above results suggested that the NiFe–ZrO_2/Cu composite catalyst prepared using the impregnation method is highly promising as a

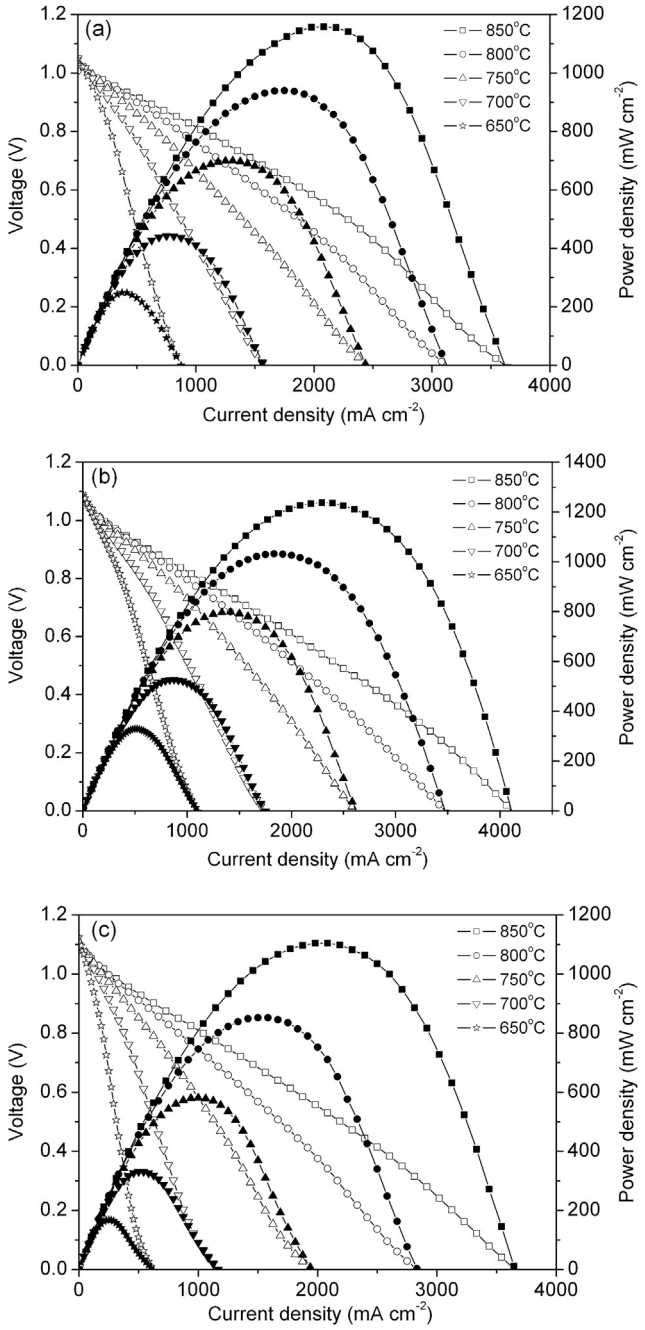

Fig. 6. *I–V* curves and *I–P* curves for the fuel cell with various catalyst layers operating on pure hydrogen at different temperatures. (a): NiFe–ZrO_2/Cu (GNP), (b): NiFe–ZrO_2/Cu (IMP) and (c): NiFe–ZrO_2/Cu (PM).

conductive catalyst layer of SOFCs for operation on methane fuel with improved coking resistance.

4. Conclusions

The current study aimed to determine the effects of preparation methods on the performance of the copper-incorporated NiFe–ZrO_2 catalyst layer for SOFCs. For the partial oxidation of methane reaction, the NiFe–ZrO_2/Cu (GNP) catalyst displayed a slightly higher catalytic activity than the NiFe–ZrO_2/Cu (IMP) and NiFe–ZrO_2/Cu (PM) catalysts. The NiFe–ZrO_2/Cu (IMP) catalyst possessed considerably higher coking resistance than the other two catalysts. Furthermore, the NiFe–ZrO_2/Cu (PM) and NiFe–ZrO_2/Cu (IMP) catalysts showed higher surface conductivities than the NiFe–ZrO_2/Cu (GNP) catalyst, comparable to those of a conventional Ni–YSZ anode, suggesting that the former two copper-incorporated catalysts had sufficient conductivity to be used as the current collector for SOFCs. When operated on CH_4–O_2 fuel, PPDs of 1080, 1011 and 1165 mW cm^{-2} were obtained by the fuel cells with the NiFe–ZrO_2/Cu (GNP), NiFe–ZrO_2/Cu (PM) and NiFe–ZrO_2/Cu (IMP) catalyst layers, respectively. However, a decrease in the operating temperature led to different power outputs. The fuel cell that contained the NiFe–ZrO_2/Cu (IMP) catalyst layer showed a much higher PPD operating on CH_4–O_2 fuel than the other two catalysts, which was

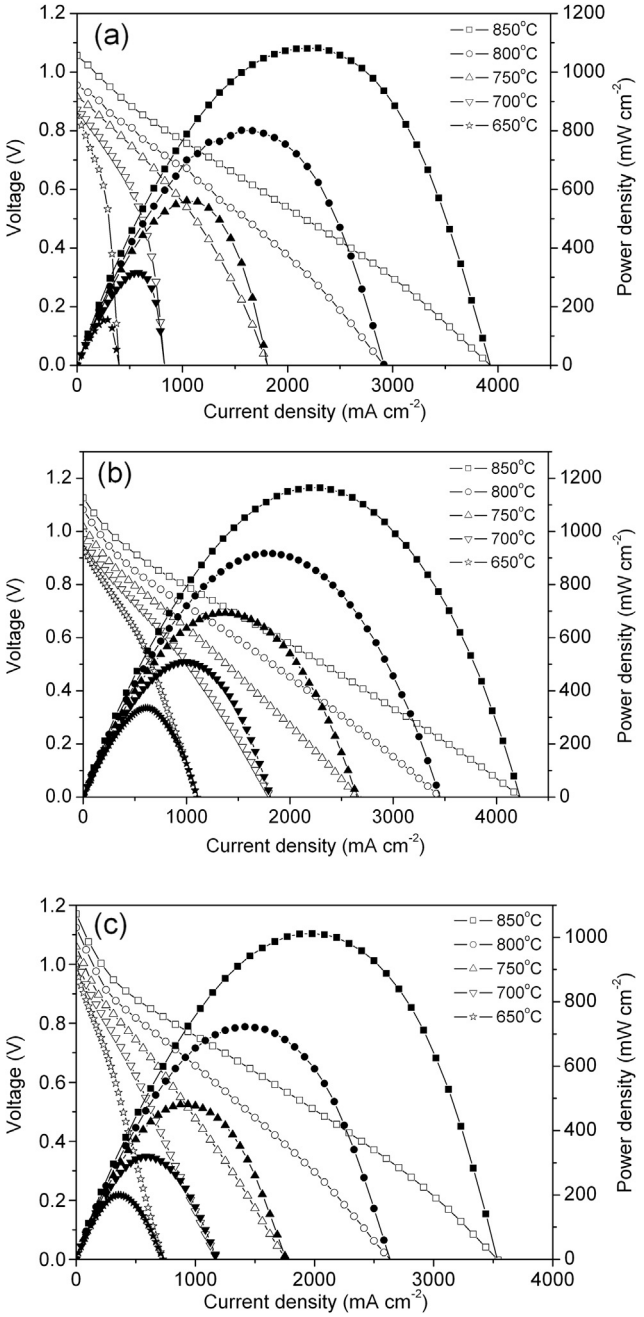

Fig. 7. *I–V* curves and *I–P* curves for the fuel cell with various catalyst layers operating on 80% CH_4 and 20% O_2 at different temperatures. (a): NiFe–ZrO_2/Cu (GNP), (b): NiFe–ZrO_2/Cu (IMP) and (c): NiFe–ZrO_2/Cu (PM).

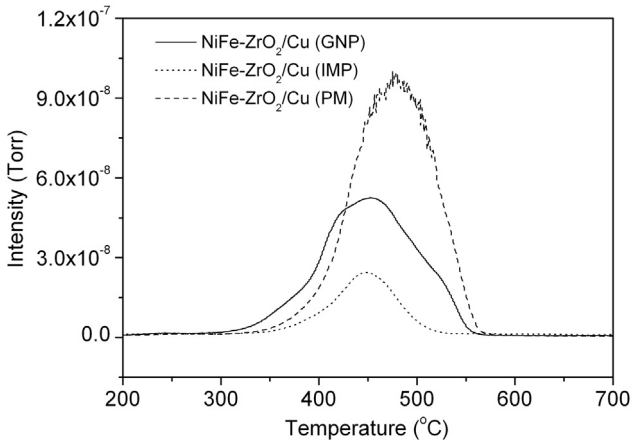

Fig. 8. O_2-TPO profiles of the NiFe–ZrO_2/Cu (GNP), NiFe–ZrO_2/Cu (IMP) and NiFe–ZrO_2/Cu (PM) catalysts after treatment in pure methane for 5 min at 650 °C.

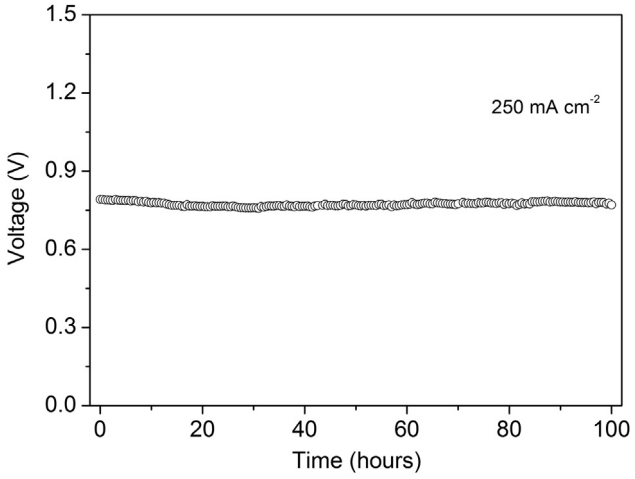

Fig. 9. The time dependence of the voltage under a specific current density (250 mA cm^{-2}) at 650 °C of the fuel cell with the NiFe–ZrO_2/Cu (IMP) catalyst layer operating on 80% CH_4 and 20% O_2 gas mixtures as fuel.

attributed to its excellent coking resistance ability towards methane. The fuel cell that contained the NiFe–ZrO_2/Cu (IMP) catalyst layer also exhibited an excellent operational stability on CH_4–O_2 fuel without any decay for 100 h. The above results indicated that the copper-incorporated catalyst prepared via the impregnation method could be used as a conductive and coking-resistant catalyst layer for SOFCs operating on methane.

Acknowledgments

This work was supported by the “National Science Foundation for Distinguished Young Scholars of China” under contract No. 51025209 and Samsung Advanced Institute of Technology project.

References

[1] S. Park, J.M. Vohs, R.J. Gorte, Nature 404 (2000) 265–267.
[2] T. Hibino, A. Hashimoto, T. Inoue, J. Tokuno, S. Yoshida, M. Sano, Science 288 (2000) 2031–2033.
[3] A. Wojcik, H. Middleton, I. Damopoulos, J. Van herle, J. Power Sources 118 (2003) 342–348.
[4] C. Su, Y.Z. Wu, W. Wang, Y. Zheng, R. Ran, Z.P. Shao, J. Power Sources 195 (2010) 1333–1343.
[5] Y.Z. Wu, C. Su, C.M. Zhang, R. Ran, Z.P. Shao, Electrochem. Commun. 11 (2009) 265–268.
[6] S.W. Tao, J.T.S. Irvine, Nat. Mater. 2 (2003) 320–323.
[7] S. Zha, A. Moore, H. Abernathy, M. Liu, J. Electrochem. Soc. 151 (2004) A1128–A1133.
[8] H. Kan, H. Lee, Appl. Catal. B Environ. 97 (2010) 108–114.
[9] H. Shimada, X. Li, A. Hagiwara, M.J. Ihara, Electrochem. Soc. 160 (2013) F597–F607.
[10] S. Song, M. Han, J. Zhang, H. Fan, J. Power Sources 233 (2013) 62–68.
[11] Y.H. Huang, R.I. Dass, Z.L. Xing, J.B. Goodenough, Science 312 (2006) 254–257.
[12] H. He, J.M. Vohs, R.J. Gorte, J. Electrochem. Soc. 150 (2003) A1470–A1475.
[13] Z.L. Zhan, S.A. Barnett, Science 308 (2005) 844–847.
[14] T. Suzuki, T. Yamaguchi, K. Hamamoto, Y. Fujishiro, M. Awanoa, N. Sammes, Energy Environ. Sci. 4 (2011) 940–943.
[15] W. Wang, W. Zhou, R. Ran, R. Cai, Z.P. Shao, Electrochem. Commun. 11 (2009) 194–197.
[16] W. Wang, C. Su, Y.Z. Wu, R. Ran, Z.P. Shao, J. Power Sources 195 (2010) 402–411.
[17] H.Y. Zhu, W. Wang, R. Ran, C. Su, H.G. Shi, Z.P. Shao, Int. J. Hydrogen Energy 37 (2012) 9801–9808.
[18] W. Wang, C. Su, R. Ran, H.J. Park, C. Kwak, Z.P. Shao, Int. J. Hydrogen Energy 36 (2011) 5632–5643.
[19] W. Wang, R. Ran, C. Su, Z.P. Shao, D.W. Jung, S. Seo, S.M. Lee, Int. J. Hydrogen Energy 36 (2011) 10958–10967.
[20] H.X. Gu, R. Ran, W. Zhou, Z.P. Shao, J. Power Sources 172 (2007) 704–712.
[21] W. Wang, C. Su, R. Ran, Z.P. Shao, J. Power Sources 196 (2011) 3855–3862.
[22] C.G. Wiegenstein, K.H. Schulz, Rev. Sci. Instrum. 68 (1997) 1812–1813.
[23] B.N. Mondal, A. Basumallick, P.P. Chattopadhyay, J. Magn. Magn. Mater. 309 (2007) 290–294.
[24] J. Zhang, Q. Wang, Y. Wang, L. Wen, C. Dong, J. Alloys Compd. 505 (2010) 179–182.
[25] M.F. Luo, P. Fang, M. He, Y.L. Xie, J. Mol. Catal. A Chem. 239 (2005) 243–248.
[26] S.D. Robertson, B.D. McNicol, H. De Bass, S.C. Kloet, J.W. Jenkins, J. Catal. 37 (1975) 424–431.
[27] P.K. Sharma, N. Saxena, A. Bhatt, C. Rajagopal, P.K. Roy, Catal. Sci. Technol. 3 (2013) 1017–1026.
[28] E. Wanzenberg, F. Tietz, P. Panjan, D. Stöver, Solid State Ionics 159 (2003) 1–8.
[29] C. Pecharroman, J.S. Moya, Adv. Mater. 12 (2000) 294–297.